Petroleum & Coal
ISSN 1337-7027

Available online at www.vurup.sk/petroleum-coal
Petroleum & Coal 56 (1) 99-109, 2014

NANOSTRUCTURED Pt/Al_2O_3 CATALYST FOR THE PARTIAL OXIDATION OF METHANE TO SYNGAS

Faranak Akhlaghian[1], Ali Mohajeri[2], Jafar Towfighi[3]

[1]Department of Chemical Engineering, Faculty of Engineering, Kurdistan University, Sanandaj, Iran;[2] Gas Research Division, Research Institute of Petroleum Industry, Tehran, Iran;[3]Faculty of Chemical Engineering, Tarbiat Modares University, Tehran, Iran

Received January 2, 2014, Accepted February 25, 2014

Abstract

Nanostructured Pt/Al_2O_3 catalysts were synthesized using sol-gel method and washcoated on a cordierite honeycomb monolith. Fresh catalysts were structurally characterized via X-ray diffraction, temperature programmed reduction, transmission electron microscopy, specific surface surface area and porosimetry techniques. The activity of the nanostructured Pt/Al_2O_3 catalyst was evaluated for partial oxidation of methane to syngas, showing stable performance of the catalyst. In the latter part of this work, a central composite design was performed to study catalytic tests. Furnace temperature, methane flow rate and methane composition in feed were considered as independent variables, whereas methane conversion and CO and H_2 selectivities were considered as responses. Empirical models of the responses were obtained, and their adequacies were assessed by analyzing of the variance. Optimal process parameters, which obtain the maximum responses, were also determined.

Keyword: Nanostructured catalyst; Partial oxidation of methane; Syngas, Catalyst stability; Optimization of process parameters.

1. Introduction

Partial oxidation of methane (POM) over catalysts based on noble metal is a promising alternative method for methane conversion to synthesis gas (a mixture of CO and H_2 or syngas). Conventional steam reforming for producing syngas is highly endothermic whereas POM is relatively a mild exothermic reaction and therefore can be considered as an energy saving method. This process takes place in the milliseconds range of contact times; therefore, it requires a smaller reactor, and reducing the cost of the plant [1- 3]. Noble metals that have been used for POM are expensive [4-5]. Platinum also has thermal stability problems [6-7].

Schicks *et al.* [7] synthesized a nanostructured catalyst for high temperature POM via a microemulsion sol-gel process. The catalyst showed high temperature stability with no measurable deactivation at high temperature POM. Sanders *et al.* [8] synthesized a structured catalyst with supporting platinum barium hexa aluminates nanocomposites over a range of conventional substrates. They evaluated the resulting catalyst for its performance in the catalytic POM into syngas. The catalyst exhibited high and stable activity.

Optimization of the process parameters is a necessary step to make the process more cost effective. Istadi *et al.* [9-10] proposed a hybrid numerical approach to develop empirical mathematical models of methane conversion and C_2 yield from the process where methane reacts with carbon dioxide (CO_2 OCM). Keyvanloo *et al*. [11-12] developed an empirical mathematical model of naphtha steam cracking using a response surface methodology and performed a multi-objective optimization for the simultaneous maximization of ethylene and propylene.

In the first part of this work, a nanostructured Pt/Al_2O_3 catalyst washcoated on a cordierite monolith was prepared using sol-gel method and characterized. The activity and stability was tested. In the latter part of this work, a central composite design was performed for the activity assessment. Empirical mathematical models of CH_4 conversion and CO and H_2 selectivities were developed. Single-response and multi-response optimization were employed to determine the optimal independent variables.

2. Experimental

2.1 Catalyst Preparation

A honeycomb cordierite monolith (Corning) with a cell density of 400 cpsi was cut into small pieces 2.54×10 mm^2 in size. Each monolith piece consisted of four channels with internal dimensions of 1×1 mm^2. This cordierite monolith was used as the catalyst substrate.

Based on the Yoldas process, aluminum isopropoxide (Merck) was added to de-ionized water. The molar ratio of aluminum isopropoxide to water was 1:100. The mixture was kept open and stirred at a constant rate at the temperature of 85°C for 45 min. At this step, by-product of the aforementioned procedure, isopropanol, was removed. Acid nitric (Merck) was then added for peptizing. The molar ratio of aluminum isopropoxide to acid nitric was 1:0.07. Hydrogen hexachloroplatinate (IV) hydrate (Merck) was dissolved in 1, 3- butanediol and a solution of 2 Wt. % of Pt was obtained. Platinum was added through this solution. The resultant solution was stirred at the constant speed at the temperature of 85°C for 24 h [13-14].

The cut pieces of monolith were washcoated with the above solution through dripping so that the solution was homogeneously dripped onto the monolith. The washcoated monoliths dried in an oven at 100°C for 12 h. Finally, the washcoated monoliths were calcined in a muffle furnace for 6 h at the temperature of 950°C.

The monolithic catalyst was immersed in a beaker of water and exposed to ultrasonic waves for 30 min. Weight loss of the monolithic catalyst showed good adhesion of the catalyst to the cordierite substrate.

Chemical analysis test of inductively coupled plasma (ICP) was performed on the catalytic monolith, parallel to the one under the activity assessment with the same load, to determine the exact load of platinum. The monolithic catalyst was dissolved in aqua regia, and the solution was placed in a microwave, after the predefined process was complete, the precipitate was separated from the solution and the content of the solution was measured by ICP spectrometry (Agilent 7500 ICP-MS instrument). The load of Pt was 0.2%. The ICP analysis repeated with Pt/Al_2O_3 powder and the corresponding load of Pt was determined to be 5.75%. The mixture of Pt and alumina gel were dried and calcined without washcoating on the monolith to prepare Pt/Al_2O_3 powder.

2.2 Characterization

The degree of crystalline order of the powder sample was assessed with X ray diffraction (XRD) at room temperature using Philips PW 1840 powder diffraction with Cu K_α radiation in the diffraction angles ranging from 2°-90°.

Specific surface area and porosity of the powder sample were obtained using an ASAP Micrometrics 2011. Before measuring nitrogen adsorption, the powder sample was degassed at 300°C for 6 h.

Transmission electron microscopy studies were performed using a Philips CM 120 instrument operated at an accelerated voltage of 100 kV. The sample was prepared by suspending a small amount of powder in an alcohol solution and then fixed on the holey carbon films supported on the copper grids.

Temperature programmed reduction (TPR) experiment was performed over the pieces of monolithic catalysts with a Micrometrics TPD/TPR 2900 apparatus. During the test, one piece of monolithic catalyst (approximately 100 mg) was placed into the apparatus. TPR profiles were recorded by heating the samples from room temperature to 600°C at the rate of 10°C/min under an H_2/Ar (5% v/v) gas flow of 40 Nl/min.

X ray photoelectron spectra were acquired with a VG Microtech XR 3E2 spectrometer equipped with an Al K_α (1486.6 eV) X ray source. The base pressure in the analysis chamber was 10^{-9} torr. The C 1s peak from carbon contamination of the sample at 284.9 eV was used as a reference for the measurements of the other binding energies.

2.3 Experimental Setup

The experimental setup consisted of mass flow controllers (Brooks 5850 E), furnace and thermocouples, a reactor, and a gas chromatograph. The monolithic catalyst was placed in a quartz reactor [4, 15]. Type K thermocouples were used to measure temperature and placed inside quartz tubes to prevent the probable contributions of thermocouples metal in the reaction.

Two thermocouples were used: one directly before and one after the monolith. Methane, nitrogen, and oxygen gas flows with high purities were controlled using the mass flow controller and then guided inside the reactor. Gas products entered the gas chromatography device (Varian CP 3800) for measuring the compositions of O_2, N_2, CH_4, CO, CO_2, and H_2.

3. Experimental Design and Numerical Methods

Central composite rotatable design (CCRD) for three factors was employed. The value of α for rotatability depends on the number of points in the factorial portion of the design, which is given by Eq. (1) [16-17]:

$$\alpha = (F)^{1/4} \qquad (1)$$

where F is the number of points in the factorial portion of the design ($F=2^k$, k denotes the number of the factors).

Because there are three factors, the F number is equal to 2^3(=8) points, subsequently, α=1.68 according to Eq. (1).

The ranges and levels used in the experimental work are presented in Table 1. All experiments were performed at atmospheric pressure, and the CH_4/O_2 ratio for all experiments was 2.0. In the experimental design, all variables were coded for statistic calculation according to Eq. (2):

$$\boldsymbol{X_i = \frac{\propto [2x_i - (x_{max} + x_{min})]}{x_{max} - x_{min}}} \qquad (\mathbf{2})$$

where X_i is the dimensionless coded value of the *ith* variable, and x_{max} and x_{min} are the highest and lowest limit of the *ith* variables, respectively.

Table 1 Experimental ranges and levels of independent variables

Factors (X)	Ranges and levels (x_i)				
	-α	-1	0	+1	+α
Furnace temperature (°C)	600	660	750	840	900
Molar composition of methane in feed (%)	10	12	15	18	20
Methane flow rate (ml/min)	60	74.1	88.5	102.9	117

The design matrix, shown in Table 2, consists of 16 sets of coded conditions expressed as the natural values. The design consists of a two-level full factorial design (2^3=8), six axial points and two central points. The sequences of the experiments were determined randomly to minimize the effects of any uncontrolled factors. These responses and factors were then modeled, providing second-order polynomial equations that predict the effects of the experimental variables and their interactions with the dependent variables. Each Y response surface, with three independent variables, is given as follows:

$$Y = b_0 + \sum_{j=1}^{3} b_j X_j + \sum_{j=1}^{3} b_{jj} X_j^2 + \sum_{i<j} b_{ij} X_i X_j \qquad (3)$$

where Y is the predicted response, b_0 is the offset term, b_j is the linear effect, b_{ij} is the interaction effect, and b_{jj} is the squared effect. In this study, CH_4 conversion and CO and H_2 selectivities were obtained as responses to these experiments. Empirical models were used for single-response and multi-response optimization. The optimization problems were solved using the Nelder-Mead simplex technique which is a standard unconstrained optimization algorithm. All the steps in this section performed in MATLAB.

Table 2 Experimental design matrix in their natural values and experimental results

Run No.	Experimental design matrix (uncoded)			Experimental Results		
	Furnace temperature (x_1)	Molar composition of methane in feed (x_2)	Methane flow rate (x_3)	X_{CH4} (%)	S_{CO} (%)	S_{H2} (%)
1	660	12	74.1	28.39	63.74	47.00
2	840	12	74.1	46.26	71.10	55.19
3	660	18	74.1	37.33	72.51	49.73
4	840	18	74.1	46.90	82.19	68.91
5	660	12	74.1	25.07	55.76	34.60
6	840	12	102.9	38.62	70.02	41.31
7	660	18	102.9	36.86	63.69	46.57
8	840	18	102.9	47.66	84.93	53.75
9	600	15	102.9	33.04	57.57	34.97
10	900	15	88.5	52.97	87.07	73.24
11	750	10	88.5	37.96	75.11	39.28
12	750	20	88.5	38.17	66.34	53.00
13	750	15	60	38.07	69	53.37
14	750	15	117	28.72	61.68	37.46
15	750	15	88.5	36.95	69.71	52.45
16	750	15	88.5	36.98	69.64	52.50

X_{CH4}: CH_4 conversion (%);S_{CO}: CO selectivity (%);S_{H2}: H_2 selectivity (%);Total pressure: 1 atm;CH_4/O_2 ratio: 2.0.

4. Results and Discussions

4.1 Catalyst Characterization

The XRD pattern of Pt/Al_2O_3 powder is shown in Fig. 1. The peaks attributed to γ-alumina (JCPDS File NO. 290069) and metallic platinum (JCPDS File NO. 040802) are marked in the figure. The XRD pattern confirms the metallic state of platinum (Pt^0).

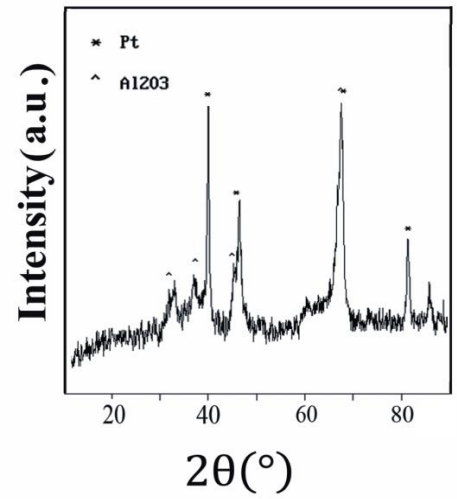

Fig. 1 XRD pattern of 5.75% Pt/Al_2O_3

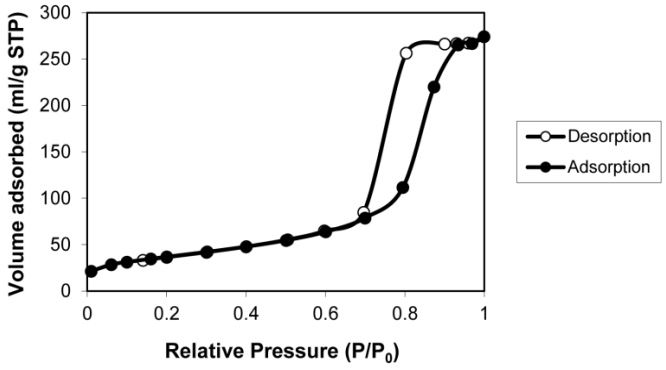

Fig. 2 Liquid nitrogen adsorption/desorption isotherm of 5.75% Pt/Al_2O_3 powder

Table 3 shows the specific surface area, average pore diameter, and pore volume of the Pt/Al_2O_3 powder. The γ-alumina phase resulted in the high surface area value.

Fig. 2 shows that there was type IV adsorption/desorption isotherm of the Pt/Al_2O_3 catalyst with type H2 hysteresis [18]. The appearance of the triangle hysteresis loop and the average pore diameter indicates mesoporosity of the Pt/Al_2O_3 powder.

Table 3.Specific surface area, average pore volume and pore diameter of 5.75%Pt/Al_2O_3 powder

Powder sample	Specific surface area (m^2/g)	Average Pore diameter (nm)	Pore volume (cm^3/g)
5.75% Pt/Al_2O_3	202.62	8.40	0.43

The BET and pore volume are calculated from the BJH adsorption isotherms (the mean pore diameter d_h is calculated assuming a cylindrical pore geometry, S_{BET} being taken as the pore surface area, $d_h=4V/S$).

TEM images of Pt/Al_2O_3 powder are shown in Fig. 3. The Pt particles (black spots) are small and well dispersed throughout the alumina matrix (grey substrate). The nanometric scaled Pt particles can easily be observed in Fig. 3.

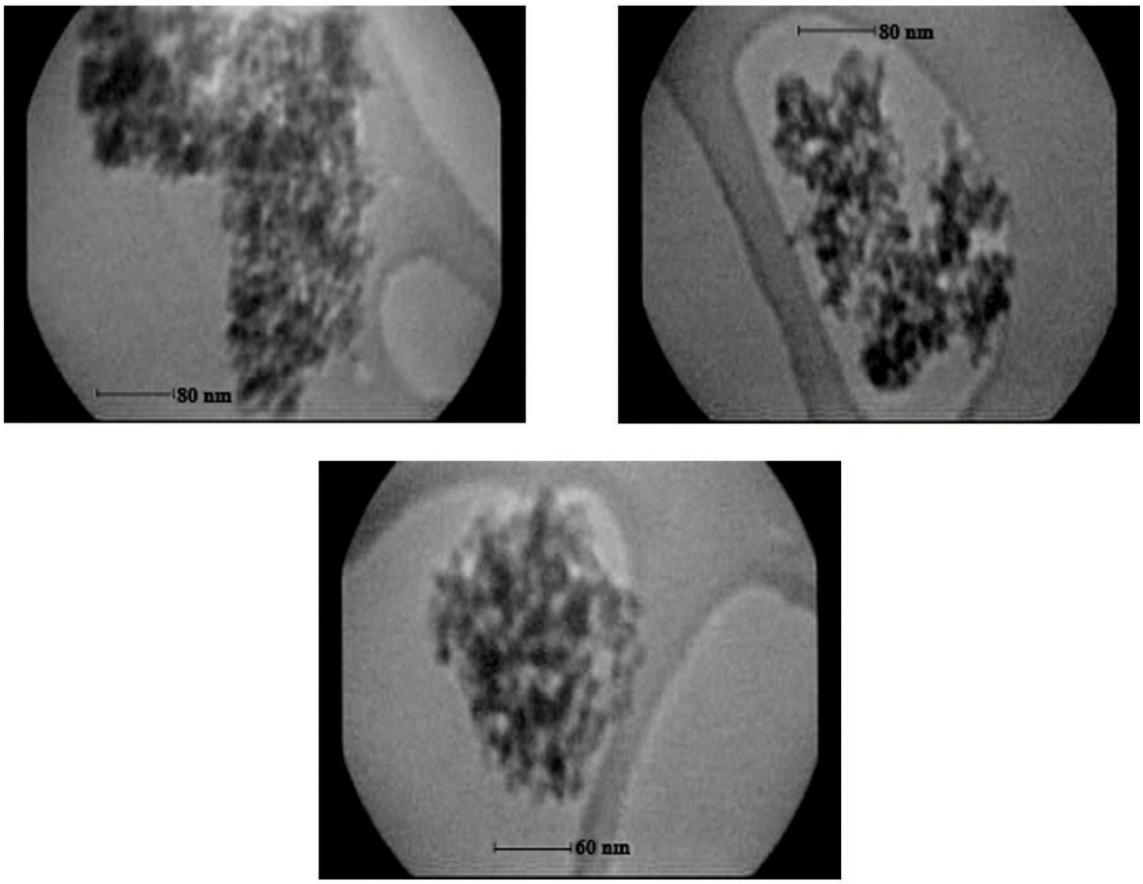

Fig. 3 TEM images of 5.75% Pt/Al_2O_3

In the TPR assay of Pt/Al_2O_3, only a small peak appeared at 397°C, which can be attributed to the reduction of Pt^{2+}. Fig. 4 shows the TPR profile of 5.75% Pt/Al_2O_3 powder. The amount of hydrogen consumption was 0.09 mmol H_2/gr of catalyst equal to 0.017 gr of Pt^{2+} /gr of catalyst (0.85% of total amount of Pt of catalyst). This result shows that the amount of Pt^{2+} is very low and that most of the Pt is in the metallic form (Pt^0).

In the XPS catalyst assessment, binding energy level of Al 2p overlapped with Pt 4f. Therefore, the binding energy levels of Pt 4d were analyzed [19-20].

Fig. 5 shows that the Pt 4d spectra of Pt/alumina/cordierite ranged from 305 to 355 eV. According to the literature, the peak at the binding energy of 314.5 eV belongs to Pt 4d5; however, for this catalyst, the peak is shifted to a lower value of 313.07 eV. This result indicates the presence of a Pt^0 species. The peak at a binding energy of 317.52 eV is ascribed to Pt^{2+}. The shoulder of this peak extending to 319.9 eV indicates that Pt^{4+}, which is a higher oxidation state of Pt, can also be present. According to the literature, the binding energy of 313.2 eV belongs to Pt 4d3 [19-20]. For this catalyst, the peak shifted to 329.45 eV,

indicating the presence of Pt^0 (metallic Pt) in the catalyst, which is in the agreement with the results of XRD and TPR.

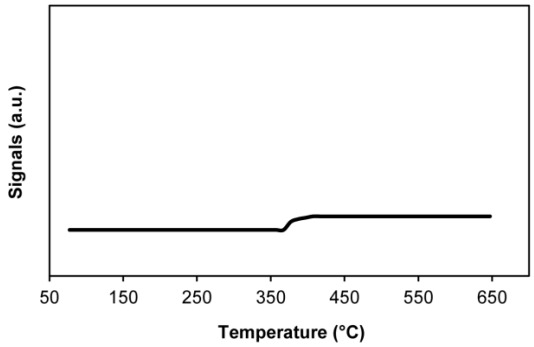

Fig. 4 TPR profile of 5.75% Pt/Al_2O_3 powder

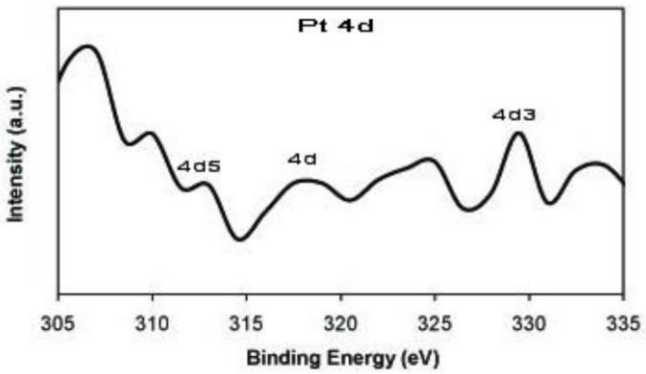

Fig. 5 Pt 4d spectra of 0.2%Pt/3.36%Al_2O_3/cordierite catalyst

4.2. Catalyst Stability

The catalyst stability was evaluated in 60-hour period test, in which the CH_4/O_2 ratio of 2.0, GHSV of 5.3×10^5 h^{-1}, furnace temperature of 750°C, methane composition of 15%, and methane flow rate of 66.3 ml/min were maintained as the assessment conditions.

Fig. 6 shows that there is no sign of deactivation in the catalytic activity over the course of the test. Stable methane conversion was approximately 37.34%, and the CO, and H_2 selectivities were 68.87% and 64.9%, respectively.

Similar tests showed no signs of deactivation. Sever sintering was expected for metal particles at very high temperature during POM; however, this catalyst showed high sintering resistance. It appears that a strong interaction between Pt nanoparticles and alumina could be the reason for this high temperature stability.

A low load of Pt, a comparable amount of activity, and a high level of stability make this catalyst a better choice, when compared with other conventional POM catalysts [6- 8].

4.3. Empirical Models

An empirical model of POM over a nanostructured catalyst, washcoated on honeycomb cordierite substrate, was developed with response surface methodology based on the design of experiments using CCRD. Note that replications were performed twice at the central points to evaluate the pure error of each measurement. Regression analyses were performed on the data of methane conversion and on the CO and H_2 selectivities, as listed in Table 2. The resulting second-order models for methane and CO and H_2 selectivities are generated in Eqs. (4)- (6):

$$X_{CH4}(methane\ conversion) = 2.28X_1^2 + 0.53X_2^2 - 1.12X_3^2 + 5.99X_1 + 1.50X_2 - 1.68X_3 - 0.10X_1X_2 - 0.82X_1X_3 + 0.12X_2X_3 + 36.89 \quad (4)$$

$$S_{CO}(CO\ selectivity) = 0.92X_1^2 + 0.36X_2^2 - 1.54X_3^2 + 8.08X_1 + 0.87X_2 - 2.58X_3 + 3.17X_1X_2 + 3.27X_1X_3 - 1.7X_2X_3 + 69.70 \quad (5)$$

$$S_{H2}(H_2\ selectivity) = -0.74X_1^2 - 2.07X_2^2 - 2.33X_3^2 + 8.10X_1 + 3.144X_2 - 5.6X_3 + 4.05X_1X_2 - 1.05X_1X_3 - 1.63X_2X_3 + 52.38 \quad (6)$$

where X1, X_2, and X_3 denote furnace temperature, methane composition, and methane flow rate, respectively.

In Eq. (4), the determination coefficient R^2 is 0.9369; in Eq. (5), it is 0.9426, and for H_2 selectivity, it is 0.913. The determination coefficients of all the models indicate good agreement between the experimental and predicted values of the fitted models.

Model accuracy was checked with variance analysis. The tabulated F-value ($F_{0.05, 6, 9}$) is 1.61 [17], and the calculated F-values of methane conversion and CO and H_2 selectivities are 9.91, 10,69 and 7.07, respectively. The calculated F-values of all models are greater than the corresponding tabulated values. The F-values show a statistically significant regression at a 5% level of significance. In this case, the null hypothesis (H_0) is rejected at a 5% level of significance based on marked F-values, thus implying that at least one of the independent variables contributes significantly to the model.

The significance of the regression coefficients was tested by Student's t-test [17]. The results are shown in Table 4. Coefficients with one factor represent the effect of the particular factor, while coefficients with two factors and those that are second-order represent the interaction between the two factors and the quadratic effect, respectively. As observed in Table 4 and according to the t-values, it is clear, for all the models, the linear term of furnace temperature (X_1) imposes a significant effect on the response, whereas the other terms are statistically insignificant. In the hydrogen selectivity model, the linear term of methane flow rate (X_3) probably has a significant effect on the response. However, the effects of other terms are not statistically significant.

Table 4 Multiple regression and significance of regression coefficients for the response models

Parameter	Term	Methane conversion model		CO selectivity model		H_2 selectivity model	
		Coefficient	t-value	Coefficient	t-value	Coefficient	t-value
b_0		36.89	13.10	69.70	21.18	52.38	10.42
b_1	X_1	5.99	5.13	8.08	5.92	8.10	3.88
b_2	X_2	1.50	1.27	0.87	0.63	3.14	1.50
b_3	X_3	-1.68	-1.44	-2.58	-1.87	-5.60	-2.68
b_{11}	X_1^2	2.28	1.72	0.92	0.60	0.74	0.31
b_{22}	X_2^2	0.53	0.40	0.36	0.23	-2.07	-0.88
b_{33}	X_3^2	-1.12	-0.85	-1.54	-0.99	-2.32	-0.98
b_{12}	X_1X_2	-0.10	-0.06	3.17	1.68	4.05	1.40
b_{13}	X_1X_3	-0.82	-0.51	3.27	1.74	-1.05	-0.36
b_{23}	X_2X_3	0.12	0.08	-1.70	-0.90	-1.63	-0.56
R^2		0.936		0.942		0.913	
R		0.967		0.970		0.955	

Three-dimensional surface plots of CH_4 conversion are observed in Fig. 7. This figure shows that an increase in the furnace temperature has a positive effect on methane conversion, whereas an increase in the methane flow rate has a negative effect.

Fig. 8 shows the contour plots of CH_4 conversion. Figure 7 indicates that at the temperature less than 750°C, an interaction exists between the furnace temperature and methane flow rate.

Figure 9 shows contour plots of CO selectivity. There is an interaction between the methane flow rate and furnace temperature on the CO selectivity. At low furnace temperatures, increasing the flow rate decreases CO selectivity, but at high furnace temperatures, increasing flow rate increases CO selectivity.

The results of the experiments (listed in Table 2 and shown in figure 6, 7, and 8) indicate that methane conversion, along with CO and H_2 selectivities increase with the furnace temperature, which is consistent with previous studies [21-22].

This characteristic indicates that the controlling step of the reaction is the kinetics of the reaction, because increasing the temperature has no effect on mass transfer.

The CO and H_2 selectivities increase with temperature, whereas CO_2 and H_2O selectivities decrease. A two-step synthesis gas production mechanism can provide an explanation. First, exothermic total combustion takes place, and the products of total oxidation (CO_2 and H_2O) are produced. Then, synthesis gas is produced through steam reforming [21-22]. Increased temperatures enhance the endothermic steam reforming of methane.

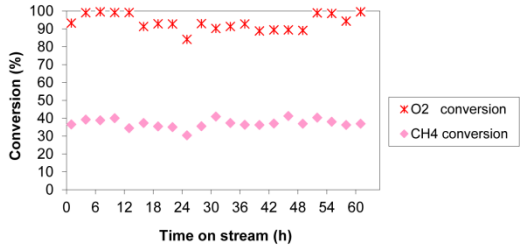

Fig. 6 Stability of methane and oxygen conversion of a 0.2%Pt/3.36%Al_2O_3/ cordierite catalytic monolith

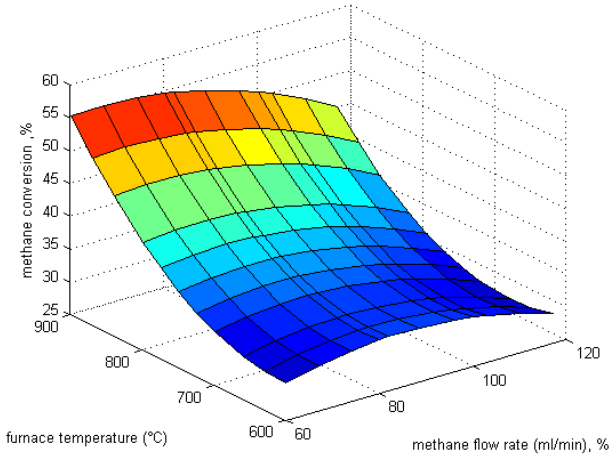

Fig. 7 Surface plot of CH_4 conversion versus the furnace temperature and methane flow rate with the molar methane composition of 15%

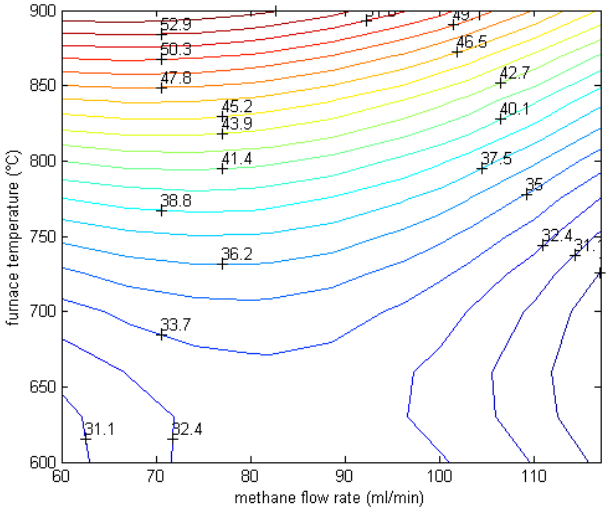

Fig. 8 Contour plot of CH4 conversion as a function of the furnace temperature and methane flow rate at a constant molar methane composition of 15%

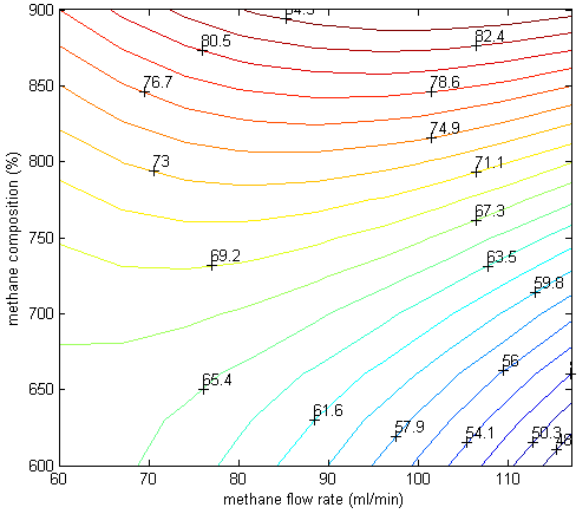

Fig. 9 Contour plot of CO selectivity as a function of the furnace temperature and methane flow rate at the constant molar composition of 15%

4.4. Optimization

For the POM optimization study, the objectives are to maximize methane conversion along with the CO and H_2 selectivities. Multi-variable single optimization was performed using the Nelder-Mead Simplex technique. Table 5 reveals the independent optimal value of methane conversion and the CO and H_2 selectivities, together with their optimal independent variables.

For a multi-response optimization technique of methane conversion with CO selectivity or H_2 selectivity, WSSOF (weighted Sum of Squared Objective Functions)is performed by varying the weighting factors (W_i) such that the sum of W_1 and W_2 is unity. The weighting factors of W_1 and W_2 correspond to the CH_4 conversion, $F_1(X)$, and the CO or H_2 selectivity, $F_2(X)$, respectively [10-12].

The locations of the optimal factors at which the corresponding responses simultaneously achieve their maximum are shown in Tables 6 and 7. Table 6 reveals that the simultaneous CH_4 conversion and CO selectivity obtained correspond to the following optimal factors: 900°C furnace temperature, 88.88 ml/min methane flow rate, and 20% molar methane composition in feed.

Table 5 Maximum of CH_4 conversion, CO, and H_2 selectivity and the location of optimal process parameters

Response	Maximum value	Location of factors for maximum responses		
		Furnace temperature (°C)	Molar methane composition in feed (%)	Methane flow rate (ml/min)
CH_4 conversion	58.94%	900	20	66.94
CO selectivity	97.33%	900	20	88.84
H_2 selectivity	89.37	900	20	60

Table 6 Simultaneous optimal multi-response of CH_4 conversion and CO selectivity

Simultaneous optimal multi-response		Corresponding weighting coefficient (W_i)
Response	Maximum value (%)	
CH_4 conversion	57.08	W_1=0.1
CO selectivity	97.33	W_2=0.9
Location of factors for simultaneous optimal-response		
Factors/independent variable		Optimal value
Furnace temperature (°C)		900
Molar methane composition in feed (%)		20
Methane flow rate (ml/min)		88.88

Table 7 Simultaneous optimal multi-response of CH_4 conversion and H_2 selectivity

Simultaneous optimal multi-response		Corresponding weighting coefficient (W_i)
Response	Maximum value (%)	
CH_4 conversion	58.75	W_1=0.1
H_2 selectivity	89.37	W_2=0.9
Location of factors for simultaneous optimal-response		
Factors/independent variable		Optimal value
Furnace temperature (°C)		900
Molar methane composition in feed (%)		20
Methane flow rate (ml/min)		60

5. Conclusion

Partial oxidation of methane was conducted over nanostructured Pt/Al_2O_3 washcoated on a honeycomb cordierite monolith. A washcoating solution was prepared based on the Yoldas process. TEM images demonstrated the dispersion of the nano scale Pt particles. The results of XRD, TPR, and XPS characterization indicated that in this catalyst, Pt is in the metallic form (Pt^0).

High temperatures stability of this catalyst was shown. Interaction between the platinum particles and aluminum support prevented Pt particles sintering. A central composite design was employed for the activity tests. The relationships between responses i.e., CH_4 conversion and CO and H_2 selectivities with three independent variables (furnace temperature, methane flow rate, and molar composition of methane of feed), were obtained. The effects of the independent variables on the process responses were investigated; temperature showed the highest effect on the responses. The maxima of the responses and optimal parameters were determined.

Acknowledgements

The financial supports of Kurdistan University, Tarbiat Modares University, and Iranian Research Institute of Petroleum Industry are gratefully acknowledged.

References

[1] Neumann, D., Veser, G.: Catalytic partial oxidation of methane in a High-Temperatured Reverse-Flow reactor, AIChE J. 2005, 51(1), 210.

[2] Scheiedernoch, R., Tischer, S., Correa, C., Deutschmann, O.: Experimental and numerical study on the transient behavior of partial oxidation of methane in a catalytic monolith, Chem. Eng. Sci. 2003, 58(3-6), 633.

[3] Chen, L., Lu, Y., Hong, Q., Lin, J., F.M.: Catalytic partial oxidation of methane to syngas over Ca-decorated-Al_2O_3-supported Ni and NiB catalysts, Appl. Catal. A: Gen. 2005, 292, 295-304.

[4] Cimino, S., Landi, G., Lisi, L., Russo, G.: Development of a dual functional structured catalyst for partial oxidation of methane to syngas, Catal. Today 2005, 105(3-4), 718.

[5] Pavolva, S.N., Sazonova, N.N., Ivanova, J.A., Sadykov, V.A., Snegurenko, O.I. Rogov, V.A., Zolotarski, I.A., Moroz, E.M.: Partial oxidation of methane to synthesis gas over supported catalysts based on Pt-promoted mixed oxides, Catal. Today 2004, 91-92, 299.

[6] Albertazzi, S., Arpentinier, P., Basile, F., Del Gallo, P., Fornasari, G., Gary, D., Vaccari, A.: Deactivation of a Pt/Al_2O_3 catalyst in the partial oxidation of methane to synthesis gas, Appl. Catal. A: Gen. 2003, 247(1), 1.

[7] Schicks, J., Neumann, D., Specht, U., Veser, G.: Nanoengineered catalysts for high-temperatured methane oxidation, Catal. Today 2003, 81(2), 287.

[8] Sanders, T., Papas, P., Veser, G.: Supported nanocomposite catalysts for high-temperature partial oxidation of methane, Chem. Eng. Sci. 2008, 142(1), 122.

[9] Istadi, Amin, N.A.S.: Optimization of process parameters and catalyst compositions in carbon dioxide oxidative coupling of methane over $CaO\text{-}MnO/CeO_2$ catalyst using response surface methodology, Fuel Process. Technol. 87(5), 449.

[10] Istadi, Amin, N.S.A.: A hybride numeriacal approach for multi-response optimization of process parameters and catalyst compositions in CO_2 OCM process over $CaO\text{-}MnO/CeO_2$ catalyst, Chem. Eng. J. 2005, 106(3), 231.

[11] Keyvanloo, K. Towfighi, J.: Comparing the catalytic performances of mixed molybdenum with cerium and lanthanide oxides supported on HZSM-5 by multiobjective optimization of catalyst compositions using nondominated sorting genetic algorithm, J. Anal. Appl. Pyrolysis 2010, 88(2), 140.

[12] Keyvanloo, K., Towfighi, J., Sadrameli, S.M., Mohmadalizadeh, A.: Investigating the effect of key factors, their interactions and optimization of naptha steam cracking by statistical design of experiments, J. Anal. Appl. Pyrolysis 2010 87(2), 224.

[13] Truyen, D., Courty, M., Alphonse, P., Ansart, F.: Catalytic coatings on stainless steel prepared by sol-gel route, Thin solid films 2006, 495(1-2), 257.

[14] Germani, G., Alphonse, P., Courty, M., Schuurman, Y., C. Mirodatos, C. : Platinum/ceria/ alumina catalysts on microstrustured for carbon monoxide conversion, Catal. Today, 2005, 110(1-2), 114.

[15] Lanza, R., J Järås, S.G., Canu, P.: Partial Oxidation of Methane over Supported Ruthenium Catalysts, Appl. Catal. A.: Gen., 2007 325 (1), 57.

[16] Box, G.E.P., Draper, N.R.: Empirical modeling-building and response surface, John Wiley & Sons, 1987.

[17] Montgomery, D.C.: Design and Analysis of Experiments, John Wiley & Sons, New York, 2001.

[18] Leofanti, G., Padovan, M., Tozzola, G., Venturelli, B.: Surface area and pore texture of Catalysts, Catal. Today 1998, 41(1-3), 207.

[19] Serrano-Ruiz, J.C., Huber, G.W., Sanchez-Castillo, M.A., Dumesic, J.A., Rodriguez-Reinoso, F., Sepulveda-Escribano, A.: Effect of Sn addition to $Pt/CeO_2\text{-}Al_2O_3$ and Pt/Al_2O_3 catalysts: An XPS, ^{119}Sn MÖssbauer and microcalorimetry study, J. Catal. 2206, 241(2), 378.

[20] Corro, G., Fierro, J.L., Odilon, V.C.: An XPS evidence of Pt^{4+} present on sulfated Pt/Al_2O_3 and its effect on propane combustion, Catal. Commun. 2003, 4(8), 371.

[21] Horn, R., Williams, K.A., Degenstein, N.J., Bitsch-Larsen, A., Dalle Nogare, D., Tupy, S.A., Schmidt, L.D.: Methane catalytic partial oxidation on autothermal Rh and Pt foams catalysts: Oxidation and reforming zones, transport effects, and approach to thermodynamic equilibrium, J. Catal. 2007, 249(2), 380.

[22] Donnazzi, A., Beretta, A., Groppi, G., Forzatti, P.: Catalytic partial oxidation of methane over 4% Rh/α-Al_2O_3 catalyst Part I: Kinetics study in annular reactor, J. Catal. 2008, 255(2), 241.

Corresponding Author :Faranak Akhlaghian, Email: Fr.Akhlaghian@uok.ac.ir, Tel.: + 98 871 666004, Fax: +98 871 666002